

Modeling of sensitivity and resolution to an included object in homogeneous scattering media and in MRI-derived breast maps

Yaling Pei and Feng-Bao Lin

**Polytechnic University, Brooklyn, NY*

*Randall L. Barbour

SUNY Downstate Medical Center, Brooklyn, NY

rbarbour@netmail.hscbklyn.edu

Abstract: We have examined the measured sensitivity and edge resolution to an included tumor in MR-derived maps of the breast exposed to NIR illumination. A large parameter space was explored, enabling a systematic examination of the influence that measurement parameters (*e.g.*, view angle, source position, wavelength) and target medium parameters (*e.g.*, breast and tumor size, background tissue properties, and tumor contrast) have on the computed responses. The significance of these findings on data collection schemes for imaging studies is discussed.

© 1999 Optical Society of America

OCIS codes: (170.3830) Mammography; (170.3660) Light propagation in tissues

References

1. S. Fantini, S. A. Walker, M. A. Franceschini, A. E. Cerussi, *et al.*, "Characterization of breast tumors by frequency-domain optical mammography," In *Advance in Optical Imaging and Photon Migration*, J. G. Fujimoto *et al.*, ed., Vol. 21 of OSA Proceeding Series (Optical Society of America, Whashington, D. C., 1998), pp. 289–293.
2. V. Ntziachristos, X. H. Ma, M. Schnell, A. Yoldh and B. Chance, "Concurrent multi-channel time-resolved NIR with MR mammography instrumentation and initial clinical results," *Ibid.*, pp. 284–288.
3. R. L. Barbour, R. Andronica, Q. Sha, H. L. Graber, and I. Soller, "Development and evaluation of the IRIS-OPTIScanner, a general-purpose optical tomographic imaging system," *Ibid.*, pp. 251–255.
4. B.W. Pogue, M. Testorf, U. L. Osterberg, and K. D. Paulsen, "Development of quantitative imaging in frequency-domain diffuse optical tomography for breast cancer detection," *Ibid.*, pp. 245–250.
5. S. B. Colak, D. G. Papaioannou, G. W. 't Hooft, M. B. van der Mark, *et al.*, "Tomographic image reconstruction from optical projections in light-diffusing media," *Appl. Opt.* **36**,180-213 (1997).
6. R. L. Barbour, H. L. Graber, J. Chang, S.-L. S. Barbour, P. C. Koo and R. Aronson, "MRI-guided optical tomography: Prospects and computation for a new imaging method," in *Computational Science & Engineering*, (Institute of Electrical and Electronic Engineerings, New York, 1995), pp. 63–76.
7. "VoxelView 2.5 User's Guide," Vital Images, Inc. www.vitalimages.com (1995).
8. H. W. Shen and C. R. Johnson, "Semi-automatic image segmentation: A biomedical thresholding approach," Technical Report UUCS-94-019, Dept. of CS, Univ. of Utah (1994).
9. D. F. Watson, "Computing the n -dimensional Delaunay tessellation with applications to Voronoi polytopes," *Computer Journal* **24**(2), 167–172 (1981).
10. N. Weatherill, and O. Hassan, "Efficient three-dimensional grid generation using the Delaunay triangulation," *Proceeding of the 1st European CFD Conference*, **1** (1992).
11. R. Beck, B. Erdmann and R. Roitzsch, "Kaskade 3.0 — An object-oriented adaptive finite element code," Technical report TR 95-4, Konrad-Zuse-Zentrum für Informationstechnik, Berlin (1995).
12. T. L. Troy, D. L. Page, D. L. and E. M. Sevick-Muraca, "Optical properties of normal and diseased breast tissues: Prognosis for optical mammography," *J. Biomedical Opt.* **3**, 342–355 (1996).
13. H. L. Graber, Y. Pei, R. Aronson, H. and R. L. Barbour, "Dependence of object sensitivity and resolution on optical thickness of scattering media," *Appl. Opt.* submitted.

1. Introduction

Most basic to any imaging method is an appreciation of the limits of sensitivity and achievable resolution. Ultimately, these are limited by the quality of the collected data. In the case of simple projection imaging, the properties of the point-spread function largely determine the sensitivity and resolution limits. For model-based tomographic imaging of scattering media, significant improvement in both quantities is possible, although in practice they are strongly influenced by a complex relationship between a host of parameters associated with the target properties (*i.e.*, target domain), conditions and quality of collected data (*i.e.*, measurement domain), and stability and accuracy of numerical methods used for image recovery (*i.e.*, analysis domain). To derive a useful tool requires suitable optimization of these parameters. In practice, assessment of the necessary tradeoffs can be complicated because of interactions among the three different parameter domains whose particulars depend on the physics of energy propagation for the problem being studied. Key to these efforts is the need to adopt methodologies that identify expected system performance under defined realistic conditions. We believe that such results can provide a guide to rational instrument development, and serve as a basis of comparison to clinical studies and an aid in test validation.

Recently a variety of instrument configurations employing optical measurement schemes have been proposed to investigate the breast. Examples include: planar compression using a raster scan method with a single detector positioned opposite a source [1], a similar geometry but with an array of sources [2], a multi-source planar radial measurement method with [3] and without [4] an adaptive measurement head, and a multi-source area detection method with a fixed cup geometry [5]. An approach we have taken to guide rational instrument development has been to use computer modeling and simulation techniques to evaluate anatomically accurate models of human tissue as defined by MR images [6]. We hold that this approach is far more cost-effective than empirically based prototype development efforts involving test measurements performed on volunteers.

As a precursor to systematically defining the dependency that each of these parameter domains has on expected image quality, in this report we have explored the dependencies that two of these domains, (*i.e.*, target properties and measurement technique), have on measures of sensitivity and edge resolution to an included object (simulating a tumor) located in a MRI-derived breast map as determined by a *simple projection*. Specifically, we have examined the inter-dependencies that measurement parameters (*e.g.*, view angle, wavelength and source location) and target parameters (*e.g.*, use of contrast agents, target geometry and size, background contrast, inclusion contrast and structural heterogeneity) have on the sensitivity and edge resolution for a defined region-of-interest (ROI). We recognize that measures of resolution derived from projection data do not coincide on a 1:1 basis to variations in resolution obtained from image reconstruction. The latter is dependent on many factors including view angle, sensitivity to ill-conditioning, computational effort, grid scale, *etc.* Nevertheless, it is frequently the case that conditions that degrade sharpness in edge spread functions seen in projection data also degrade the achievable resolution in the corresponding image data. It follows that specification of conditions that optimize the measurement sensitivity and edge resolution should allow for recovery of improved image quality.

Our study is divided into two parts: exploration of homogeneous models with a centered inclusion simulating a tumor, and examination of anatomically accurate optical (AAO) breast models, defined by MRI data, containing a centered "tumor." We include the homogeneous model primarily to differentiate the influence of geometry factors from effects of internal contrast features on the measured response. Its simplicity also facilitates focused laboratory investigations on phantoms for the purpose of verifying potentially interesting system performance features.

2. Methods

2.1 Segmentation of MRI Breast Maps and FEM Mesh Generation

MR images of the breast were obtained using a GE Signa MRI system. The fast spin echo technique (TR = 4000 ms, TE = 112 ms, 3 mm thickness) was used, with and without fat and water suppression. A series of 24 sagittal images was obtained, and each image was subsequently converted into coronal views using the VoxelView image display program [7]. The MRI breast maps were segmented using a semi-automatic image segmentation code provided by Chris Johnson from the University of Utah [8]. This code permits identification of user-defined outer and inner boundaries using a cubic spline data-fitting method. Figure 1(a) shows the representative coronal-view map (displayed at low resolution) used in these studies. Figure 1(b) shows the corresponding representative finite element mesh employed, in which a central inclusion simulating a tumor was introduced. The boundary geometries of the two maps differ because the external boundary of the breast was extended to conform to a circular geometry in the FEM model. This simplification was adopted to reflect the expected geometry that would exist for measurements of the breast using a newly constructed imager [4].

Three different tissue types are identified: adipose (dark region in MRI map, red color in FEM model), parenchyma (light region in MRI map, green color in FEM model) and the centrally positioned tumor shown in the FEM map (blue color). This location was selected because it represents the region most difficult to detect. The extended region was assigned coefficients corresponding to adipose. The segmented image served as the input file for FEM mesh generation. The mesh generation code, also provided by C. Johnson, uses the Delaunay tessellation algorithm originally proposed by Watson [9] and later extended by Weatherhill [10].

The number of points and elements on the mesh used in the different models varied with breast size. For small diameters, the number of the points and elements was on the order of 1,500 and 3,000, respectively. For large diameters, these values are increased by as much as a factor of 15. An adaptive uniform refinement method was used to improve the efficiency of the FEM calculation for large-diameter maps [11]. It is worth noting that whereas a variety of breast maps have been examined, here we present results on a single MRI map. Thus, the internal structural configuration of the background tissue is identical for all breast/tumor composite geometries explored. We do this for the purpose of differentiating the influence that variations in background/tumor contrast have on the measured parameters from effects caused by variations in the composite breast/tumor geometry.

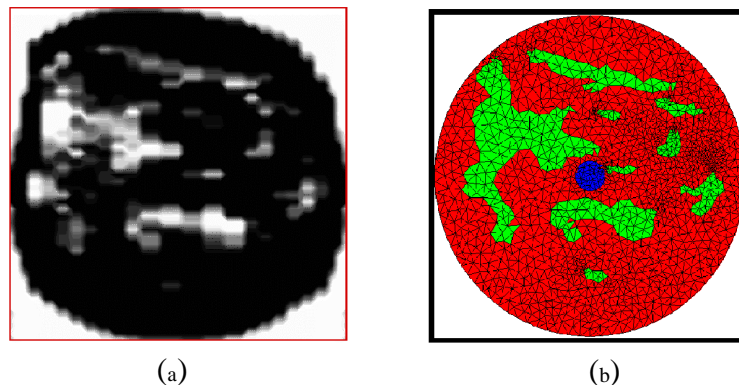


Fig. 1. (a) Image of a coronal slice of a breast derived from MRI maps; (b) FEM model used for computation.

2.2 Forward Model and Data Acquisition Geometry

In our study, we modeled light propagation in breast tissue as a diffusion process. For a domain Ω having a boundary $\partial\Omega$ and a DC point source, this is represented by the expression:

$$\nabla \cdot [D(\mathbf{r})\nabla u(\mathbf{r})] - \mu_a(\mathbf{r})u(\mathbf{r}) = -\delta(\mathbf{r} - \mathbf{r}_s), \quad \mathbf{r} \in \Omega \quad (1)$$

where $u(\mathbf{r})$ is the photon density at position \mathbf{r} , \mathbf{r}_s is the position of the point source, and $D(\mathbf{r})$ is the position-dependent diffusion coefficient, which is related to the absorption coefficient $\mu_a(\mathbf{r})$ and reduced scattering coefficient $\mu'_s(\mathbf{r})$ by

$$D(\mathbf{r}) = \frac{1}{3[\mu_a(\mathbf{r}) + \mu'_s(\mathbf{r})]}. \quad (2)$$

Photon density values at the detectors were computed by applying Dirichlet boundary conditions on an extrapolated boundary. Depending on the breast size, the sources and detectors were positioned 1–2 transport mean free pathlengths below the extended surface. Solutions to the diffusion equation were computed using the KASKADE adaptive finite element method [11]. This is a publicly available code suitable for the solution of partial differential equations in one, two or three dimensions, using adaptive finite element techniques. For our purposes, we modified the basic code to enable solutions to the diffusion equation with a point source. Figure 2 illustrates the data acquisition geometry employed. The arrows in the figure show two different locations of sources used for the reported studies. Whichever of the two sources is adopted, the position of the detector corresponding to the source location is designated as 0° . The angular increment of the detectors was made in steps of 10° proceeding in the clockwise direction.

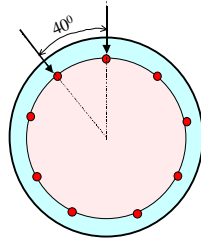


Fig. 2. Data acquisition geometry for a full tomographic view with 36 detectors in a uniform ring geometry (only 9 detector are shown in the figure). The arrows show two different source locations used for the reported results.

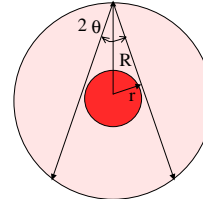


Fig. 3. Illustration of parameters used to define edge resolution. See text for details.

2.3 Definition of Sensitivity and Edge Resolution

We define measurement sensitivity as the relative change in detector response between a defined background and target medium (background + embedded objects). The background medium refers to cases where only the adipose and parenchyma tissues are present. The target medium refers to cases where a tumor has been introduced into the background. We use $u(\mathbf{r})_t$ and $u(\mathbf{r})_b$ to represent the computed detector response from the target and background medium, respectively. Then sensitivity is defined as:

$$\delta_u = \frac{u(\mathbf{r})_b - u(\mathbf{r})_t}{u(\mathbf{r})_b} \quad (3)$$

and identifies the relative influence the added tumor has on surface detector responses.

Measures of edge resolution were obtained by computing the edge spread function, corrected for the expected influence of the tumor geometry. This is defined as the excess of the full-width at half-maximum (FWHM) of the sensitivity curve above its theoretical minimum value, *i.e.*, $EFWHM = FWHM - FWHM_{geom}$, in which $FWHM_{geom} = 2\sin^{-1}(r/R)$, where r and R respectively are the radii of the centered inclusion and of the medium, as shown in Figure 3. Therefore, a decrease in EFWHM signifies an improved resolution obtained, whereas an increase in EFWHM means a loss of resolution. We introduce this correction factor in order to differentiate variations in the edge-spread function caused by changes in the dimension and properties of the background medium from changes in tumor size. In the absence of this correction, comparisons between media having different tumor sizes could be ambiguous. For example, certainly it is the case that the width of the edge spread function will increase with increasing tumor size even in a non-scattering medium. As discussed later, while this definition is valid, it is correct in *absolute* terms only in cases of comparisons between breast maps having the same diameter. On the other hand, in comparisons made involving maps of different diameters, a variation in the EFWHM is evidence of a change in the edge resolution relative to the size of the medium.

2.4 Parameter Space

We have examined the dependence of detector sensitivity to the included tumor and its derived edge resolution on four of seven principal parameters associated with the measurement and target domains directly, and, because of known relationships, by inference for the other three parameters. Those directly examined were variations in breast and tumor size, and background tissue and tumor contrast, as well as the influence of view angle and source position. Inferred parameters include the impact of structural heterogeneity, choice of illuminating wavelength and use of contrast agents. In each case, a range of parameter values was explored in an effort to better define their influence on the computed sensitivity and edge resolution.

Table 1 lists the diameters of the breast maps and tumors explored. These values were selected on the basis of the expectation that tumors can be located almost anywhere in the breast from near the nipple to the chest wall, and that breast and tumor size obviously vary. For each of the seven breast diameters examined, we additionally explored five different cross-sectional areas occupied by the tumor.

Table 1: Diameters of breasts and embedded tumors

Case #	Breast Diameter (cm)	Tumor Diameters (cm)				
		Corresponding to Ratio of Cross-Sectional Area of Tumor to Breast Size				
		0.0625 %	0.25%	1%	2.25%	4%
I	16	0.4	0.8	1.6	2.4	3.2
II	12	0.3	0.6	1.2	1.8	2.4
III	10	0.25	0.5	1.0	1.5	2.0
IV	8	0.2	0.4	0.8	1.2	1.6
V	6	0.15	0.3	0.6	0.9	1.2
VI	4	0.1	0.2	0.4	0.6	0.8
VII	2	0.05	0.1	0.2	0.3	0.4

Table 2 defines the optical coefficients assigned to an embedded tumor. The values selected were based primarily on reports in the literature regarding observed optical properties of excised normal and cancerous breast tissue [12]. In some cases, a more extended range was

adopted to explore the potential influence of contrast agents. For each of the composite breast/tumor sizes considered, we evaluated the effect that variations in tumor contrast have on sensitivity and edge resolution. This parameter was subdivided into three different contrast ranges. In two of these the scattering contrast was varied in the presence of moderate and high, but in either case fixed, absorption levels, and the third varied the absorption was varied in the presence of an expected, fixed scattering value. In total, seven different contrast levels were explored. The range of contrast values assigned to the background tissues is shown in Table 3. Here, we also explored three different ranges of coefficient values. These correspond to variations in the background absorption and scattering values of fat, and in the scattering value of the parenchymal tissue. For comparative purposes we also explored the homogeneous state, as representing the lower limit of contrast variation for the background tissues. In all, eight different background types were explored for each of the previously mentioned tumor contrast values. In total, the complete parameter matrix explored amounted to nearly 2600 cases for each source location examined. Of these, the majority of cases explored involved situations where the embedded tumor had higher coefficient values compared to the back-ground medium. It deserves emphasis that whereas we have explored other MRI breast maps, all results reported here for inhomogeneous media are derived from a single MRI map.

Table 2: Optical properties of tumor tissue

Group	Case #	μ_a (cm ⁻¹)	μ_s' (cm ⁻¹)
(A)	5, 6, 7	0.08	40, 20, 10
(B)	1, 2, 3	0.2	40, 20, 10
(C)	7, 3, 9	0.08, 0.2, 0.4	10
(D)	4, 8	0.2, 0.08	5

Table 3: Optical properties of background tissue

Group	Case #	Adipose		Parenchyma	
		μ_a (cm ⁻¹)	μ_s' (cm ⁻¹)	μ_a (cm ⁻¹)	μ_s' (cm ⁻¹)
Homogeneous	1	0.04	10	0.04	10
(A)	2, 3, 4	0.02, 0.04, 0.08	10	0.08	7
(B)	3, 7, 8	0.04	10, 15, 25	0.08	7
(C)	5, 6	0.04	10	0.08	15, 25

Legend for Tables 2 and 3: Values listed within each group are the respective optical properties for the cases examined.

3. Results

3.1 Limiting case of contrast variation in breast maps—homogeneous background

3.1.1 Influence of Target Size

The angular dependence of sensitivity to the tumor on the size of the homogeneous background (*i.e.*, breast) for a fixed inclusion (tumor) contrast value and fixed ratio of inclusion area to target area is shown in Figure 4. The target diameter was varied between 2 and 16 cm to cover the expected range of diameters in the vicinity of the nipple and chest wall. Contrary to what one might expect, we observe in all cases studied that an *increase* in

the total optical thickness of the medium (*i.e.*, corresponding to an increase in target size), significantly *enhances* the maximum relative intensity change observed at larger angular distances from the source. At intermediate angular distances, a biphasic response is observed. Here, we define total optical thickness as the physical diameter of the medium multiplied by the sum of the absorption and scattering coefficients. For a homogeneous medium this has a unique value. For heterogeneous media the value will depend on the chosen transect. Also shown in this Figure is the seemingly counterintuitive finding of a reduction in the width of the sensitivity response curve with increasing target size. This indicates that an improvement in edge resolution accompanies the enhancement in sensitivity seen with an increase in the total optical thickness. It's worth noting that these effects are not widely appreciated, although as shown elsewhere [13], they are predictable from theoretical considerations. Also, recall that because the comparison in sensitivity is between maps of different size, the enhancement in edge resolution seen is in relative terms. These responses are quantified in more detail in the next Figure.

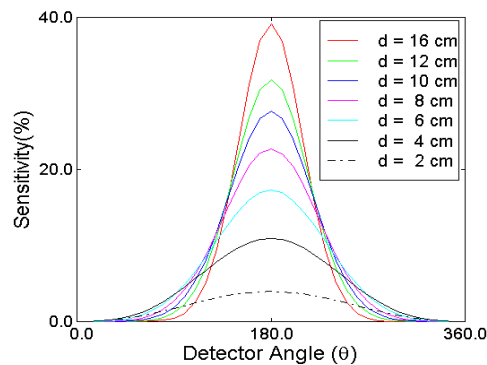


Fig. 4. Percent change in sensitivity versus view angle for different target sizes, with Case 3 tumor contrast and tumor size of $r = 1\%$, embedded in a homogeneous background medium.

3.1.2 Effect of Composite "Breast/Tumor" Size on Sensitivity and Edge Resolution

Further examination of the above-described phenomenology is shown in Figures 5(a)–(b) and 6(a)–(b). Here we have computed the sensitivity of a detector to the added tumor positioned 180° from the source (Figure 5) and the corresponding EFWHM (Figure 6), as a function of the composite breast/tumor geometry, for a fixed tumor contrast. A comparison of results in Figures 5(a) and 6(a) shows that an increase in the ratio of the cross-sectional area of the tumor-to-breast size for a fixed breast diameter increases sensitivity significantly, especially

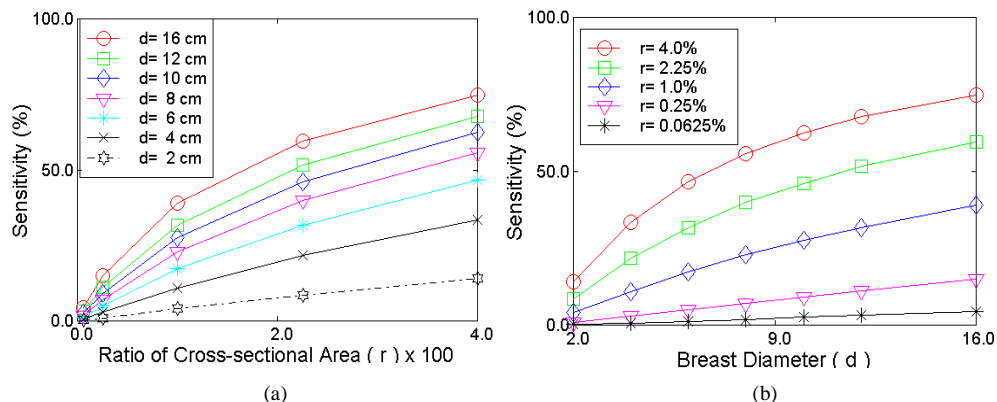


Fig. 5. Percent change in sensitivity versus (a) the cross-sectional area ratio for different breast diameters and (b) the breast diameter for different cross-sectional area ratios, for a Case 1 background medium (homogeneous) and Case 3 tumor contrast for a detector at 180° from the source.

for larger breast sizes (*cf.* Figure 5(a)), and improves edge resolution slightly (*cf.* Figure 6(a)). Results in Figures 5(b) and 6(b) demonstrate the corresponding response to variations in the breast diameter for fixed values of the area ratio. Again, a positive correlation is seen between sensitivity and target size when either one of the size parameters is fixed. Interestingly, the maximum rate of sensitivity change occurs when extreme values of the target geometry are paired (*i.e.*, breast and tumor size). Thus, the greatest change in sensitivity values occurs with large breasts containing small tumors (a clinically interesting case) (Figure 5(a)), and small breasts containing large tumors (Figure 5(b)). These findings indicate that sensitivity responses do not simply scale with target size.

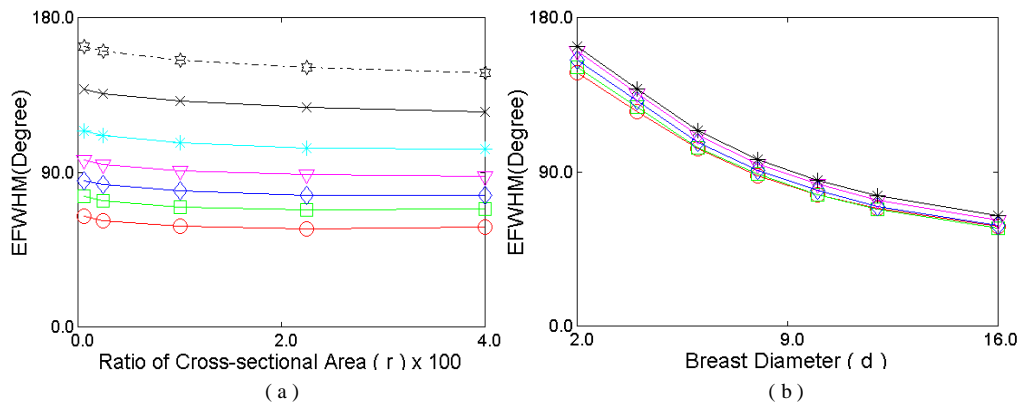


Fig. 6. EFWHM versus (a) the cross-sectional area ratio for different breast diameters and (b) the breast diameter for different cross-sectional area ratio with Case 1 background medium and Case 3 tumor contrast at 180° view angle. Definition of symbols is given in Fig. 5.

3.1.3 Influence of Composition of Target Geometry and Tumor Contrast on Sensitivity vs. Edge Resolution

The results shown in Figures 7(a)–(c) plot the EFWHM versus sensitivity response for a detector positioned 180° from the source, as functions of breast size, tumor-to-breast area ratio and tumor contrast, for the different tumor contrast groups. In Figures 7(a) and 7(b) the absorption coefficient for the tumor is fixed at 0.08 cm⁻¹ and 0.2 cm⁻¹, respectively, and the scattering coefficient varies from 10 to 40 cm⁻¹. In Figure 7(c) the scattering coefficient of the tumor is fixed at 10 cm⁻¹ and the absorption coefficient varied from 0.08 to 0.4 cm⁻¹. Shown are the responses for three different area ratios (labeled A, B, C, where A corresponds to 0.0625% (red), B to 1.0% (green), and C to 4% (blue)), as a function of breast diameter. For each line drawn, the sensitivity increases monotonically with increasing breast diameter, while at the same time the EFWHM value monotonically decreases. Inspection of this six-dimensional data set reveals the following. Most striking is the strong dependence of edge resolution and sensitivity to the tumor on breast size, especially for the smaller tumors. In this case, an increase in breast size preferentially enhances edge resolution, independent of tumor contrast. Increasing tumor size (groups A–C) when the breast size and tumor contrast values are fixed primarily enhances sensitivity, although some enhancement in edge resolution is observed for larger tumors. Comparing results in Panels (a)–(c) illustrates the effect of varying tumor contrast. Results in Panel (a) show that at moderate absorption values (*i.e.*, 0.08 cm⁻¹), increasing the scattering contrast of the tumor preferentially enhances edge resolution for small breast sizes, while improving sensitivity for larger breast sizes. This differential response is most noticeable for breasts containing larger tumors. Results in Panel (b) show that the sensitivity enhancement seen in large breasts when the scattering contrast of the tumor is increased is completely abolished upon increasing the absorption contrast of the tumor to 0.2 cm⁻¹. This shows that under the conditions examined, a four-fold enhancement

in scattering contrast of the tumor has no additional influence on its detectability. Results in panel (c) show that the greatest improvement in sensitivity is observed upon an increase in the

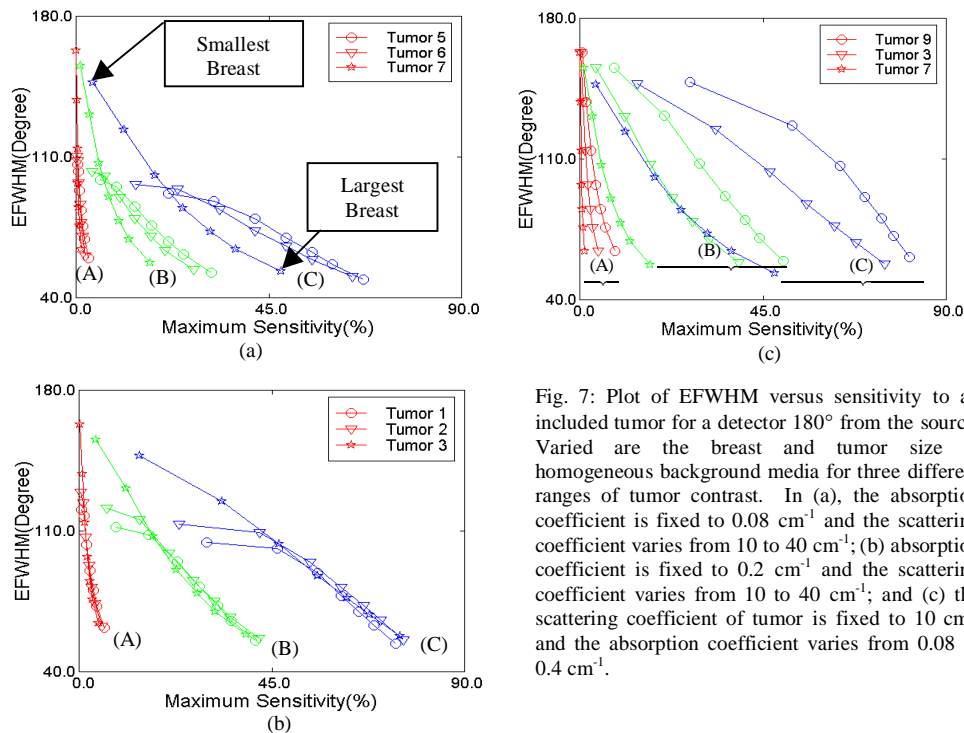


Fig. 7: Plot of EFWHM versus sensitivity to an included tumor for a detector 180° from the source. Varied are the breast and tumor size in homogeneous background media for three different ranges of tumor contrast. In (a), the absorption coefficient is fixed to 0.08 cm^{-1} and the scattering coefficient varies from 10 to 40 cm^{-1} ; (b) absorption coefficient is fixed to 0.2 cm^{-1} and the scattering coefficient varies from 10 to 40 cm^{-1} ; and (c) the scattering coefficient of tumor is fixed to 10 cm^{-1} and the absorption coefficient varies from 0.08 to 0.4 cm^{-1} .

absorption of the tumor, with the largest effect occurring with larger tumors.

3.2 Inhomogeneous Background (AAO Breast Model)

3.2.1 Effect of Increased Background Scattering

In this section we show results obtained from the AAO maps. The point of these studies is to determine if the presence of an inhomogeneous background can appreciably influence the sensitivity to and edge resolution of the included tumor, relative to the homogeneous case. Results shown in Figure 8 illustrate the effect that an increase in the difference between scattering coefficients of adipose and parenchyma tissue has on sensitivity, for the case of a small tumor (0.25% ratio of cross-sectional area) embedded in a large breast (16 cm). Specifically shown are responses seen for Groups B and C background media, which differ in the direction of the scattering contrast between the adipose and parenchymal tissues. For comparative purposes, the response seen for a homogeneous background also is shown. The most noticeable effect of background heterogeneity is a shift in the angle at which the greatest sensitivity to the tumor is observed. Interestingly, the direction of this shift depends on the algebraic sign of the difference between the background tissues' scattering coefficients. The angle of maximum sensitivity is $>180^\circ$ when the adipose is more strongly scattering than the parenchyma, and $<180^\circ$ when the parenchyma is the more strongly scattering tissue. The ratio of the maximum sensitivity value to the sensitivity at precisely 180° can be greater than 2:1, a result that highlights the influence that restricted-view measurements can have on measurement sensitivity for inhomogeneous media. Also seen in the Figure is a marked reduction of the EFWHM for the medium having the largest scattering contrast between adipose and parenchyma, especially for the Type-6 background, indicating improved edge resolution. Not shown are results of similar analyses where the tumor size and contrast value

were varied as a function of background tissue contrast. In cases involving comparisons between media with similar tumor-to-breast area ratios, the influence of variations in tumor contrast, for a specified background, were mainly quantitative in nature. That is, in situations where the measured sensitivity to the included tumor varies in manner shown in Figure 8, the observed response was largely independent of tumor contrast. This indicates that the observed behavior is primarily a function of the *background* contrast. Quantitatively, reduction in the absorption or scattering contrast of the included tumors predictably reduces measurement sensitivity. The influence of breast size on the angular response function is shown subsequently.

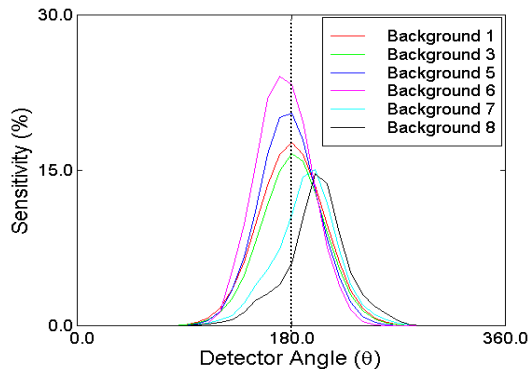


Fig. 8. Percent change in sensitivity versus view angle for different background media with a breast size of $d = 16$ cm, tumor size of $r = 0.25$ %, and Case 1 tumor contrast.

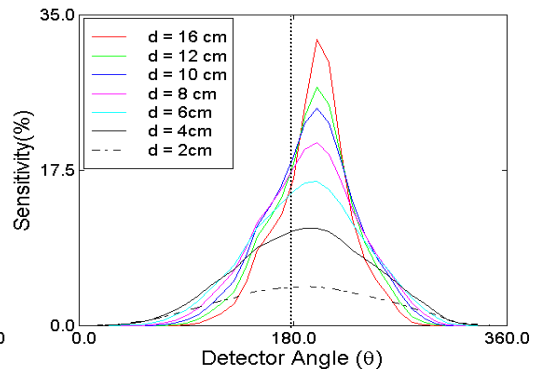


Fig. 9. Percent change in sensitivity versus view angle for different breast sizes, with Case 3 tumor contrast and tumor size of $r = 1\%$, embedded in Case 6 background medium

3.2.2 Influence of Breast Size

The results in Figure 9 show the effect on sensitivity of varying the breast size while holding the tumor-to-breast area ratio fixed, for a selected inhomogeneous background medium (*i.e.*, Case 6 background). A similar plot for the homogeneous background case was shown in Figure 4. Comparison reveals that whereas the edge resolution also improves with increasing breast size, its angular dependence is not a simple function of breast size. This absence of linear scaling between measured response and target geometry can be seen more clearly by comparing the sensitivities observed at 180° and at 200° , as a function of the composite

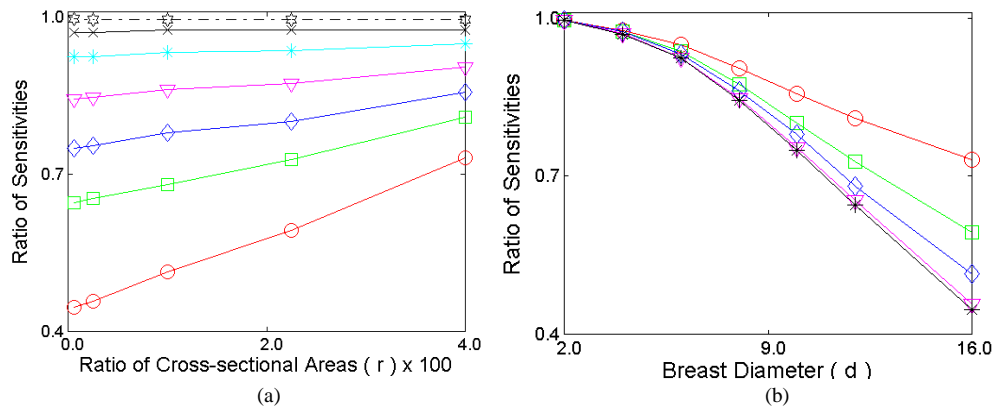


Fig. 10: Ratio of sensitivity at 180° view angle to that at 200° , versus (a) the cross-sectional area ratio for different breast diameters and (b) the breast diameter for different cross-sectional area ratio with Case 6 background tissue and Case 3 tumor contrast. Definition of symbols is given in Fig. 5.

breast/tumor size. These results are shown in Figures 10(a) and 10(b). In Panel (a) we see a strong, nearly linear, dependence of angular sensitivity on tumor size for large-diameter breasts but very little dependence for small-diameter breasts, even though the exact same inhomogeneous background structures are present. Panel (b) further shows that, in addition to this lack of scaling, the angular sensitivity dependence varies with tumor size, with the greatest dependence observed in the case of the smallest tumor embedded in a large breast.

3.2.3 Influence of Source Location

The results in Figures 11(a) and 11(b) show the dependence of the maximum detector sensitivity to the tumor on source location (0° vs. -40°), as a function of the tumor cross-sectional area ratio and the breast diameter, for background medium 6. This comparison is made to model how the source location influences the expected sensitivity of measurement for an inhomogeneous medium, as a function of the composite target geometry. Inspection of the figure reveals trends similar to those observed in Figure 10. Thus, whereas it is to be expected that varying the source position can influence measurement sensitivity for an inhomogeneous medium, what is not obvious is that the magnitude of the differential response is itself dependent on the composite target geometry. The form of this dependence reveals an absence of scaling in sensitivity as a function of composite target geometry, even though identical background structures are present.

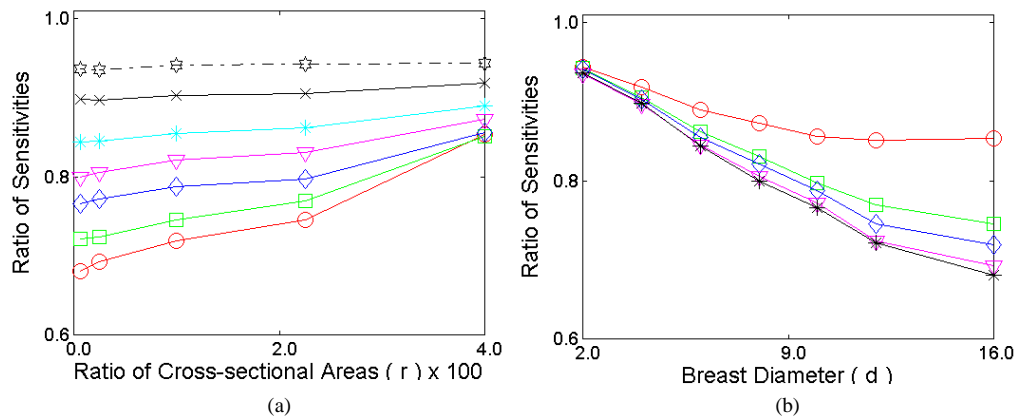


Fig. 11. Ratio of the maximum sensitivity caused by source 1 ($\theta = 0^\circ$) and source 2 ($\theta = -40^\circ$) versus (a) the cross-sectional area ratio for different breast diameters and (b) the breast diameter for different cross-sectional area ratio with case 6 background tissue and case 3 tumor contrast. Definition of symbols is given in Fig. 5.

3.2.4 Comparison of Sensitivity Dependence of MRI Breast Map to Homogeneous Background

Results in Figures 8–11 identified the sensitivity dependencies of various measurement configurations for a fixed structural heterogeneity, as a function of background contrast and composite target geometry. To complete our understanding, it is useful to isolate the influence of structural heterogeneity *per se*. This was investigated by comparing the measured responses for the case 6 background to a homogeneous background medium (case 1), as a function of composite target geometry, for a detector positioned opposite the source. Figure 12 shows the result for the case of type-3 tumor contrast. In Panel (a), we see that compared to the homogeneous case, the influence of structural heterogeneity on the detectability of the tumor varies strongly with the breast size. For small-diameter breast maps, the presence of added contrast between the parenchyma and adipose tissues reduces sensitivity to the tumor. However, the opposite effect is seen for larger diameter breasts, even

though an identical structural heterogeneity and contrast difference is present in all cases. This is further demonstration of an absence of scaling in the measured response with target size. Panel (b) shows a similar dependence when tumor size is varied.

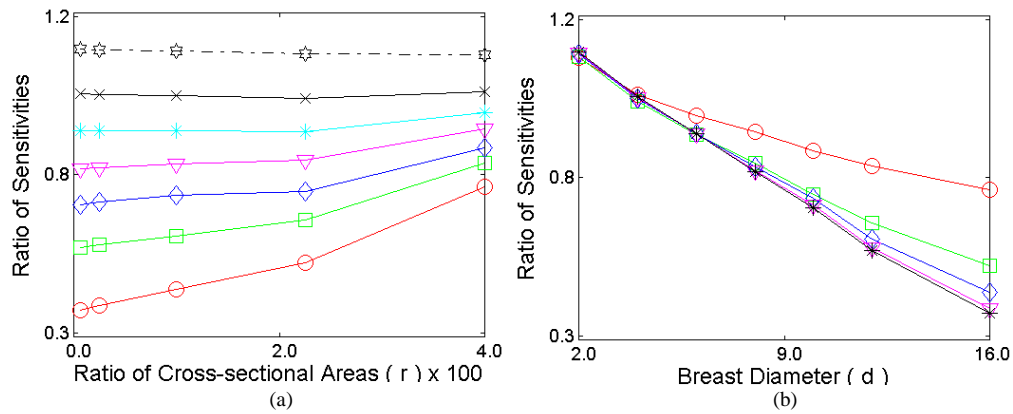


Fig. 12. Ratio of sensitivity change of case 6 background medium to homogeneous background medium (case 1) versus (a) the cross-sectional area ratio for different breast diameters and (b) the breast diameter for different cross-sectional area ratio with case 3 tumor contrast at 180° view angle. Definition of symbols is given in Fig. 5.

3.2.5 Influence of Composition of Target Geometry and Tumor Contrast on Sensitivity vs. Edge Resolution

The results in Figures 13(a)–(c) show the influence of variations in target geometry on the EFWHM and sensitivity at 180° , for the three tumor contrast ranges and a selected

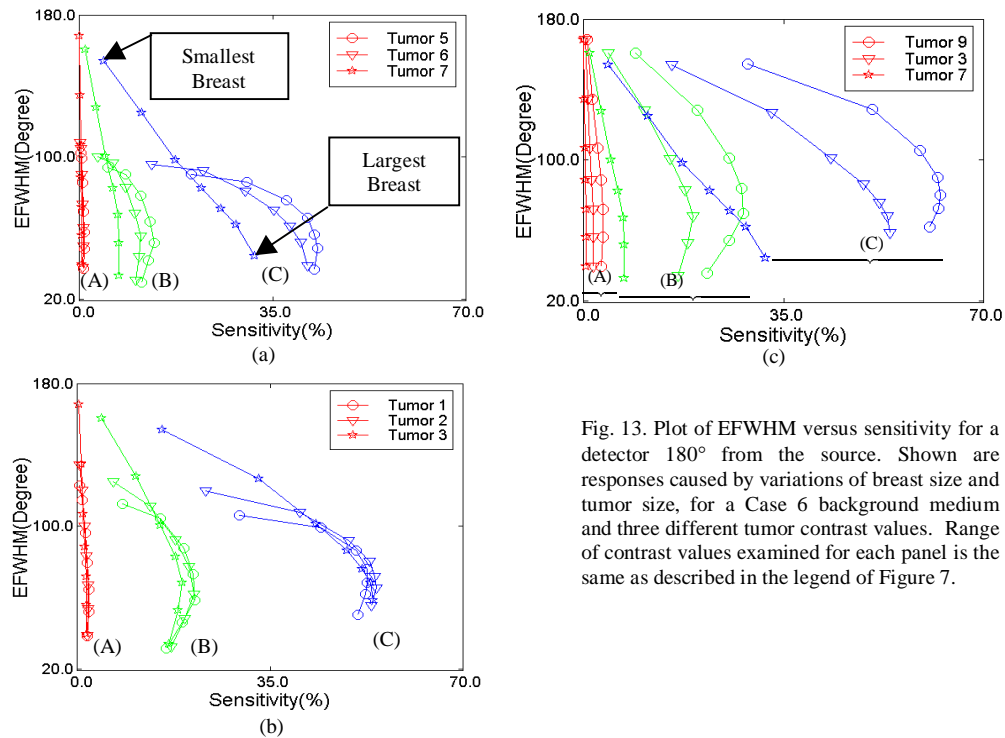


Fig. 13. Plot of EFWHM versus sensitivity for a detector 180° from the source. Shown are responses caused by variations of breast size and tumor size, for a Case 6 background medium and three different tumor contrast values. Range of contrast values examined for each panel is the same as described in the legend of Figure 7.

inhomogeneous background (*i.e.*, type 6). A similar study for a homogeneous background is shown in Figures 7(a)–(c). Comparison of data in both sets of Figures reveals that while qualitative similarities are present, overall a more complex response is seen in the inhomogeneous case. Most notable is that portions of some of the EFWHM *vs.* sensitivity relations are not single-valued functions, revealing that in these cases maximum sensitivity is achieved at some intermediate breast size. Also different is the loss of edge resolution with increasing tumor size, especially in the case (panel (c)) of an increase in the value of the tumor absorption coefficient. It is worth noting that results presented in this figure do not coincide with the position of maximum sensitivity, which as shown in Figure 9, occurs at $\sim 200^\circ$ from the source. A similar analysis at this view angle (results not shown) produced trends closer to those observed for a homogeneous medium. This suggests that background heterogeneity *per se* does not fundamentally limit the achievable edge resolution and sensitivity, but instead alters the location where they can be attained.

3.2.6 Response to Reduced Contrast Tumors

The results presented in the preceding figures emphasize mainly the influence that the various parameters have on the computed responses for tumors having contrast values greater than those of the surrounding background medium. In Figure 14 we examine the corresponding responses for a case in which the included tumor is more weakly scattering than the background, for different breast sizes, and compare this to the homogeneous case. Overall, we see that in many cases a more complex profile is observed, the trend favors improved sensitivity and improved edge detection with increased breast size.

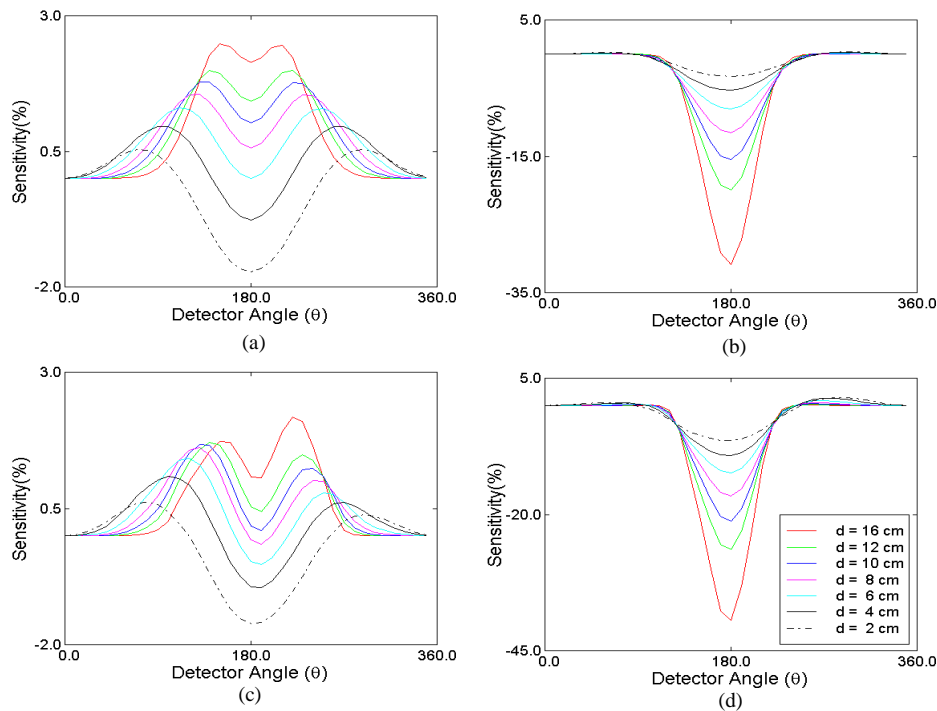


Figure 14: Percent change in sensitivity versus view angle for different breast diameters, with case 8 tumor contrast and tumor-to-breast area ratio $r = 1\%$, embedded in (a) homogeneous, (b) case 4, (c) case 5 and (d) case 8 background media, respectively. The legend shown applies to all panels.

3.3 Summary of the Principal Results

An important phenomenon observed in the results presented is that for any tumor-to-breast area ratio, tumor contrast, and background medium contrast, the maximum sensitivity and edge resolution to the included tumor both increase significantly as the breast diameter increases. Also observed is that increasing tumor size, for a fixed tumor contrast and breast size, increases sensitivity to the tumor and, to a lesser extent, its resolution (*cf.* Figures 6, 7 and 13). In addition, increasing absorption contrast of the tumor alone increases sensitivity, but does not improve resolution (*cf.* Figures 7, 13). We also observed that the influence of varying the scattering contrast of the tumor on sensitivity and resolution is a function of composite target size as well as of the absorption contrast of the tumor (*cf.* Figures 7, 13). For small breasts, sensitivity and resolution are improved simultaneously as the scattering contrast of the tumor increases, but there is a larger change of sensitivity for small breasts with a large tumor. For large breasts the responses of edge resolution and sensitivity is different, such that increases in the scattering contrast of the tumor improves sensitivity alone, but only with tumors having moderate absorption contrast. In all, a consistent finding throughout all the variations explored is the absence of scaling of the measured response with target size. Specifically, we mean that trends observed in edge resolution and sensitivity as a function of tumor contrast, size and background contrast do not extrapolate to media of larger sizes, even though the exact same distribution of internal contrast and relative tumor size to background medium is present. These findings not only provide a comprehensive understanding of expected measurement performance associated with the two types of parameter spaces explored, (*i.e.* measurement and target domains), but also provide a guide to identifying the optical measurement strategies required to obtain optimal sensitivity and resolution to included objects. In the following, we extend these observations and discuss complementary strategies that can optimize achievable sensitivity and resolution.

4. Discussion

In this report we have systematically explored the parameter domains associated with the target properties and measurement conditions, for the purpose of gaining insight into the relationships between these domains and their possible influence on the design of practical imaging systems. Two critical parameters that should be kept in mind when designing such systems are expected limits on sensitivity and resolution. Without a doubt, an important factor influencing these limits will be the view angle of measurement. In the case of imaging studies on the breast several options are available, some of which have been adopted [1-5], but without rigorous proof that these are best suited for achieving optimal sensitivity and resolution.

One design in particular that has been implemented is a raster scan with a single detector positioned 180° opposite the source, with the breast subjected to mild planar compression [1]. While compression of the breast will improve signal levels, this will be at the expense of a restricted view. Results in Figure 9 show that depending on the optical properties of the background tissues and their distribution in relation to an ROI, sensitivity to a centrally located structure can vary several-fold over an angle of 20°. Since detailed knowledge of underlying structural heterogeneity of the breast is unknown *a priori*, the influence of such structures on sensitivity can be expected to vary significantly. At a minimum, this observation suggests that the presence of heterogeneous backgrounds in the breast will severely limit efforts to obtain reproducible results from measurements employing restricted views. This would be especially true should serial measurements be performed, in which case the plasticity of the breast would surely undermine efforts to reproduce precise positioning of the tissue. Because background heterogeneity can shift the location where optimal sensitivity is achieved, our results suggest that improved reproducibility should be achievable using measurement schemes that employ broader views. The difficulty with this

approach is that it may limit the ability to use planar compression schemes. As indicated, while it clear that compression of the tissue will improve signal levels, it is worth examining whether this is accompanied by expected improvements in sensitivity and resolution. Although planar compression geometries were not specifically investigated in this study, we believe that comparison of results from the different breast sizes can nevertheless provide insight into the expected influence of such geometries on these parameters.

Because the internal features of the different breast models studied are identical, to a first approximation comparison of results for different model diameters is equivalent to imposing a radial compression on the tissue. Table 4 lists results derived from Figures 5 (a)–(b) and 6 (a)–(b), where the expected influence of a radial compression maneuver on sensitivity and edge resolution of the tumor is examined assuming different compression responses of an included tumor. For simplicity, expected out-of-plane effects of tissue–tumor compression are ignored. Considered is a large breast (16 cm) containing a tumor whose size (1.6 cm) is 1% of the total cross-sectional area ratio. These results show that use of compression techniques is always accompanied a loss of resolution due to reduced breast size, while its effect on sensitivity depends on the degree of compressibility of the tumor with respect to the surrounding tissue. In the case where the tumor has similar compressibility to the surrounding media, radial compression of the tissue to 10 cm diameter causes a 29% and 35% loss of sensitivity and edge resolution, respectively. These values compare to corresponding declines of 16% and 34% for the case of partial tumor compression, and to a 25% *gain* in sensitivity coupled with a 31% *loss* of resolution for an incompressible tumor. These results show that tissue compression *per se* does not guarantee improvement in sensitivity and resolution, and not infrequently can make matters worse.

Table 4. Influence of a radial compression maneuver on sensitivity and edge resolution

Items	Before Compression	After Compression		
		1.0 (Proportionately Changed)	1.4	1.6 (Completely Unchanged)
Breast Diameter (cm)	16	10		
Tumor Diameter (cm)	1.6	1.0 (Proportionately Changed)	1.4	1.6 (Completely Unchanged)
Tumor-to-Breast Area Ratio (%)	1	1	1.96	2.56
Maximum Sensitivity (%)	39.1	27.6 (↓29.4%)	33.0 (↓15.6%)	49.0 (↑25.3%)
Resolution (EFWHM) (Degrees)	58.36	78.92 (↓35.2%)	78.11 (↓33.8%)	76.73 (↓31.48%)

As mentioned, an important matter related to instrument design is the view angle of measurement. Several groups have reported instrument designs that restrict measurement of the exiting optical signal to the location opposite the source. A critical issue influencing the performance of such systems is limits on edge resolution and sensitivity to a selected ROI. We have observed that enhancement of both can be achieved upon an increase in the size of the medium, which is equivalent to an increase in its total optical thickness. While such an increase will reduce observable signal levels, the relatively high intensities of light that can be directed to tissue without causing damage suggests that this tradeoff can be made over a selected range, up to the limit of photon deprivation. It is useful to consider strategies whereby this could be effectively accomplished.

One approach would be to immerse a target in a scattering medium, thereby extending its boundary. In this case the optodes would not be in contact with the tissue, rendering the measurement susceptible to motion artifacts. Even if this could be overcome,

there would likely be a tradeoff between increased resolution and sensitivity. This follows because extension of the external boundary would reduce the area ratio of an ROI, and, as shown in Figure 5, this could reduce sensitivity to the ROI. It would be better to achieve an effective increase in optical thickness throughout the medium. While it is evident that one cannot physically enlarge the tissue, a “virtual enlargement” can be accomplished by simply illuminating the tissue under study with light of a shorter wavelength. Since this would increase the total optical thickness without a change in physical size, an improvement in EFWHM in absolute terms would be expected. In the limit, it would be desirable to vary the wavelength of light in accordance with the distance between a source and detector, such that a nearly constant total optical thickness is achieved for all source/detector pairs. Thus, for a detector opposite the source, wavelengths in the NIR region could be employed, followed by detection of more blue-shifted signals by detectors. Selection of the illuminating wavelength range could be adjusted in accordance with the physical size of a target medium. For instance, for examination of large diameter breasts, more red-shifted wavelength ranges could be employed, whereas for smaller breasts the wavelength range would be relatively blue-shifted. It worth noting that this scheme could be influenced by skin color, especially for measurements using wavelengths shorter than 650 nm. The absorption profile of melanin can severely attenuate wavelengths of light in the visible region, thus reducing the dimensions within which acceptable signal levels can be acquired.

While the described multi-wavelength approach could complicate data acquisition and analysis schemes, it is worth noting that, as shown in Figure 4, a nearly ten-fold increase in sensitivity is observed upon an eight-fold increase in optical thickness. As an alternative, a simpler scheme, and one easily implemented, is shown Figure 15. Here, we seek to employ a

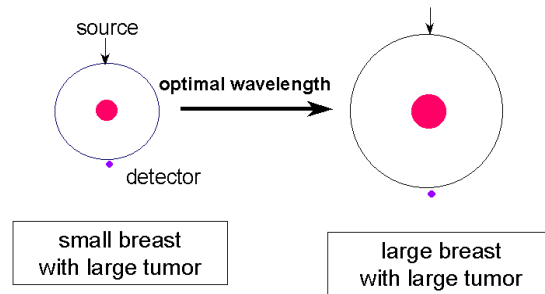


Fig. 15. Optimal wavelength approach

single or a few illuminating wavelengths. An optimal wavelength is one for which acceptable S/N levels are maintained while at the same time the greatest possible optical thickness is attained. While this method could be adapted to measurement schemes using planar

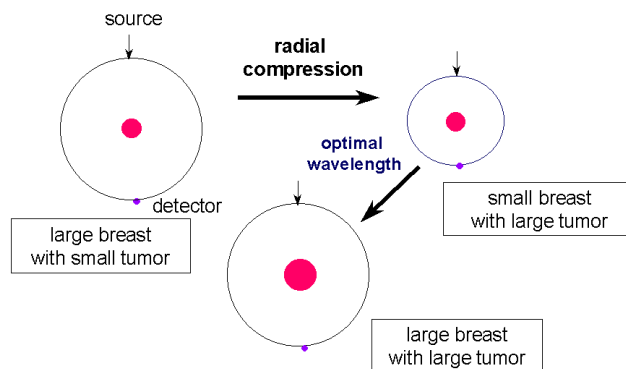


Fig. 16. Combination of radial compression and optimal wavelength approaches

compression, as mentioned, this can compromise the attainable view angle. Better might be to employ a radial compression approach. This would preserve a large view angle while permitting implementation of some form of optimal wavelength scheme. This approach is illustrated in Figure 16. In the example given, a large breast containing a small tumor is under examination. By exerting mild radial compression, the diameter of the breast will be reduced, thereby increasing available signal levels. Depending on the compressibility characteristics of the tumor, the resultant state may well produce an enhancement in sensitivity, but resolution could suffer, at least in relative terms. However, by adjusting the illumination wavelength, the total optical thickness can be increased, thereby improving both sensitivity and resolution in absolute terms.

Influence of Contrast Agents. While use of contrast agents *per se* was not examined in this study, insight regarding their expected effectiveness can be derived on the basis of the range of tumor contrast levels studied. Contrast agents are traditionally employed to enhance measurement sensitivity. Our study indicates that: (i) contrast agents used for enhancing the absorption coefficient of the tumor can increase sensitivity but do not improve edge resolution for almost all breast/tumor sizes studied; (ii) contrast agents used to enhance the scattering coefficient of a tumor improve both sensitivity and resolution in the case of a small breast. For a large breast, the response observed is mainly dependent on the absorption contrast. In the case of modest tumor absorptions, enhancement of scattering contrast in the tumor improves sensitivity. This effect, however, is completely abolished at higher absorption levels and is independent of tumor size (*cf.* Figure 7, 13). Overall, it would appear that the optimal conditions for tumor detection will benefit from the appropriate selection of optimal wavelengths and contrast agents matched to breast size.

Acknowledgments

This work was supported in part by NIH grant no. RO1-CA66184.